South African Journal of Botany 149 (2022) 632–645

Contents lists available at ScienceDirect

South African Journal of Botany

journal homepage: www.elsevier.com/locate/sajb

Potential topoisomerases inhibitors from *Aspergillus terreus* using virtual screening

Eman Zekry Attia[a,*], Basma Ali Khalifa[b], Gehan M. Shaban[b], Mohamed N. Amin[c], Lina Akil[d], Ibrahim Khadra[d], Ahmed A. Al Karmalawy[e], Radwan Alnajjar[f,g], Marco Y.W. Zaki[h], Omar M. Aly[i], Mo'men H. El-Katatny[b], Usama Ramadan Abdelmohsen[a,j,*]

[a] *Department of Pharmacognosy, Faculty of Pharmacy, Minia University, Minia 61519, Egypt*
[b] *Department of Botany and Microbiology, Faculty of Science, Minia University, Minia 61519, Egypt*
[c] *Biochemistry Department, Faculty of Pharmacy, Mansoura University, Mansoura 35516, Egypt*
[d] *Strathclyde Institute of Pharmacy & Biomedical Sciences, University of Strathclyde, Glasgow G4 0RE, United Kingdom*
[e] *Department of Pharmaceutical Medicinal Chemistry, Faculty of Pharmacy, Horus University-Egypt, New Damietta 34518, Egypt*
[f] *Pharm D, Faculty of Pharmacy, Libyan International Medical University, Benghazi, Libya.*
[g] *Department of Chemistry, University of Cape Town, Rondebosch 7701, South Africa*
[h] *Department of Biochemistry, Faculty of Pharmacy, Minia University, Minia 61519, Egypt*
[i] *Department of Medicinal Chemistry, Faculty of Pharmacy, Port Said University, Port Said 42515, Egypt*
[j] *Department of Pharmacognosy, Faculty of Pharmacy, Deraya University, New Minia, Minia 61111, Egypt*

ARTICLE INFO

Article History:
Received 30 October 2021
Revised 23 May 2022
Accepted 22 June 2022
Available online 1 July 2022

Edited by: Dr. S.O Amoo

Keywords:
Anti-topoisomerase
Artemisia arborescens
Aspergillus terreus
Cytotoxic activities
Docking
Molecular dynamics
LC-MS profiling

ABSTRACT

Cancer is appraised as one of the predominant reasons for demise worldwide. Owing to the continued resistance to the anti-topoisomerases, the worldwide challenge is the discovery of new drugs and maintenance their topoisomerase sensitivity. Therefore, the main goal of this work is to assess the potential anti-cancer effect of the ethyl acetate extracts derived from different broth media of the endophytic *Aspergillus terreus* AArEF2 isolated from *Artemisia arboresscens* L. versus HepG-2 and MCF-7 cell lines and to estimate the ability of the most potent cytotoxic extract to inhibit topoisomerase I and II enzyme activity. The findings revealed that the ethyl acetate extract afforded from the modified potato dextrose broth (MPDB) media displayed the highest cytotoxic activities with IC_{50} values of 7.92 and 8.53 μg/mL towards HepG-2 and MCF-7 cell lines, respectively and showed substantial inhibition towards topoisomerase I and II with IC_{50} values of 8.76 and 2.83 μg/mL, respectively. HPLC-ESI-HRMS analysis of such extract annotated fifteen metabolites belonging to various classes, some of which were reported for their cytotoxic activities. Regarding docking analysis, most compounds showed strong conformational energies higher than positive control drugs, particularly averantin (**12**) and asterredione (**14**), which demonstrated promising interaction abilities with Topo I and Topo II binding sites, respectively, emphasizing probable involvement of such compounds to the noteworthy cytotoxic potentials of the ethyl acetate extract of MPDB media. Also, molecular dynamics simulation has been done to confirm the docking results. These findings might point up the probable chemotherapeutic applications of *Aspergillus terreus* AArEF2 isolated from *A. arboresscens.*

1. Introduction

Cancer is reported as one of the considerable global causes of death due to a rising rate of clinical annual reported cases (Mathers and Loncar, 2006). Owing to the high rate of cancer mortality, a worldwide challenge to find out chemotherapeutics emanated from natural sources, and new scaffoldings that enhance chances of acquiring new binding process or recording novel targets, is one strategy to treat cancer (Krushkal et al., 2021). Numerous chemotherapeutics display proliferative toxicity to the normal cells causing adverse effects and they are often less operative towards various cancer types (Sak, 2012). Consequently, seeking for new high efficacy chemotherapeutics becomes a challengeable task for many researcher groups (Uzma et al., 2018).

DNA topology is maintained through DNA topoisomerases I & II, which have a substantial role in numerous essential processes inside the cell, viz. replication and transcription of DNA, formation of mitotic chromosome, recombination of DNA, and splicing of pre-mRNA (Wang, 2002). The appropriate function of topoisomerases has

* Corresponding authors at: Department of Pharmacognosy, Faculty of Pharmacy, Minia University, Minia 61519, Egypt.
E-mail addresses: eman_zekry@mu.edu.eg (E.Z. Attia), usama.ramadan@mu.edu.eg (U.R. Abdelmohsen).

https://doi.org/10.1016/j.sajb.2022.06.051
0254-6299/

a great importance in all cell operation, because any impairment of their function throughout the time of cell division will result in the destruction of the DNA, and thus, programmed-cell apoptosis will be induced . Consequently, they become the target of several scientific research groups worldwide (Malonne and Atassi, 1997). Normal healthy cells show low expression activity of human topoisomerases, while various rapidly dividing cancerous cells display high activity of such enzymes, therefore selective action of compounds acting as topoisomerase inhibitors has been taken in considered (Buzun et al., 2020; Siwek et al., 2014). Topoisomerase I (Topo I) manages the breaking and reconnecting of a single strand of a DNA duplex to relax the topological stress. So, the mechanism of Topo I inhibitors is relied on the entanglement of the DNA covalent complex created by Topo I, preventing complex break up, as a result, DNA strands are persistently disturbed, the cell cycle is arrested, and programmed cell death-apoptosis is induced (Champoux, 2001). While, Topoisomerase II (Topo II) relaxes the double helices of DNA by scissoring and constraining both strands. Topo II inhibitors are classified to Topo II poisons and catalytic inhibitors. Topo II poisons make DNA strands breakdowns, either by indorsing the development of covalent Topo II-DNA cleavage complexes, or by inhibiting constrain of the broken strands (Nitiss, 2009a). High levels of Topo II are observed in numerous types of cancers, therefore, its expression level is used as a diagnostic marker in many tumors (Nitiss, 2009b). These observations highlight targeting Topo II at the rapidly dividing cancerous cells. Several topoisomerase inhibitors have been approved from the FDA like camptothecin (CPT), as Topo I inhibitor, along with etoposide and doxorubicin as Topo II inhibitors (Baldwin and Osheroff, 2005; Champoux, 2001). Owing to the growing resistance to the known topoisomerase inhibitors, continuous seeking for new, highly efficient, and more selective alternative therapeutics is, therefore, insistently warranted (Rasheed and Rubin, 2003).

Plants are considered a great reservoir for a huge number of microorganisms that symbiotically live within plants, known as endophytes (Gouda et al., 2016). The isolated natural components from endophytic fungi reveal various bioactivities like anticancer, antimicrobial, antiviral, and antioxidant potential (Jalgaonwala et al., 2017). Natural components, characterized in the endophytic fungal extracts, are contemplated a continuous source of alternative chemotherapeutics, which attract the attention of modern medicine to explore anticancer agents with less adverse reactions (Prajapati et al., 2021).

Drug discovery from natural sources faces some considerable obstacles, viz. difficulty of the isolation of pure components due to high intricacy of the crude extracts, and sometimes presence of bioactive components in low abundances (Singh et al., 2016). Therefore, LC—HRMS based-metabolomics has recently been a prominent strategy to comprehensively characterize the metabolites in bioactive crude extracts and target promising metabolites related to the certain biological potential before starting large scale extraction for the isolation and purification of the bioactive components, which consume time and money (Sashidhara and Rosaiah, 2007). It can annotate the known natural constituents (untargeted) and point out the new ones (targeted) saving the time consumed in the separation and purification of known, but non-bioactive metabolites, from an investigated extract (Corley and Durley, 1994).

On the other hand, computational chemistry is one of the most important ways of drug discovery and development nowadays. It saves more time and effort in the long way of novel drug approval (Elmaaty et al., 2022; Hamed et al., 2021b). Molecular docking and molecular dynamics are considered to be the most applied computational techniques to describe and evaluate the binding modes and interactions of the studied molecules toward a specific receptor (Elebeedy et al., 2021a, 2021b).

In the light of the previously mentioned data, *Aspergillus terreus* AArEF2 cultivated from healthy leaves of *Artemisia arborescens* L. was investigated to find out the most proper media, which produced cytotoxic metabolic compounds acting as human topoisomerases inhibitors, by using LC-ESI-HRMS based-metabolomics and virtual screening.

2. Materials and methods

2.1. Materials and reagents

The chemicals used in such study were all of analytical grade and purchased from Sigma (USA), Merck (Germany), and SD Fine Chemicals (India).

2.2. Plant samples

The healthy fresh leaves of *Artemisia arborescens* L. were gathered from the Botanic Garden of Botany and Microbiology Department, Faculty of agriculture, Assiut University, Assiut, Egypt, and confirmed by Prof. Mahmoud A. H. Abdou, Department of Horticulture, Faculty of Agriculture, Minia University, Minia, Egypt. A voucher specimen of the plant was preserved in the herbarium of Pharmacognosy Department, Faculty of Pharmacy, Minia University, Minia, Egypt. Its registration number is Mn-Ph-Cog-054. The fresh plant specimens were reserved in the laboratory and treated within 8 hr.

2.3. Identification of the endophytic fungal isolate

Identification of the fungal endophyte isolated from the leaves of *A. arborescens* L. were brought about via the same procedure reported by Attia et al. (2020). The morphological characterization of the fungal isolate was carried out in the centre of Mycology, Assiut University, Assiut Egypt. The colony attributes were based on the examination on PDA media (Andrews and Pitt, 1986; Barnett and Hunter, 1972).

2.4. Molecular identification and phylogenetic analysis

The isolated fungal strain was characterized taxonomically through extraction of its genomic material of the DNA, then PCR magnification and sequencing internal transcribed spacer (ITS) region of the isolated fungus were performed by the universal primers ITS1 and ITS4. The Blast approach in National Center for Biotechnology Information (NCBI) was utilized to match the sequence to the database of the GenBank to detect the closest allied species with very analogous sequence to the magnified one. Finally, MEGA7 software was used to achieve the multiple sequence configuration and phylogenetic analysis (Alhadrami et al., 2021; Kumar et al., 2016).

2.5. Fermentation in liquid medium

The isolated strain *A. terreus* AArEF2 was cultured on several types of media, followed by liquid-liquid extraction with ethyl acetate (EtOAc). Sabouraud Broth (SAB), Malt Extract Broth (MEB), Rice Extract Broth (REB), modified Rice Extract Broth (MREB) and modified potato dextrose broth (MPDB) were used separately to culture the isolated fungal strain in Erlenmeyer flasks (2 L), each contain 400 mL of the above mentioned media. The modified media involve, along with their main components, the following ingredients: 0.5 g peptone 0.8 g yeast extract, 3 mg NH_4 (SO_4), 2 g KH_2PO_4, 0.5 g Mg So_4. Each flask was incubated statically at 20 °C ± 2 for 30 days. Subsequently, 100 mL EtOAc were added to all flasks to terminate the fermentation process. The fermented broth was subsequently centrifuged (6000 rpm, 15 min, 4 °C), then filtered to remove the wet mycelia. While, each obtained filtrates (300 mL) was extracted by liquid-liquid extraction with 250 mL EtOAc three times. Each afforded EtOAc solution was, afterwards, concentrated by rotary evaporator

under vacuum pressure to get a semisolid brown residue (50 mg), which was kept at 4 °C for further cytotoxic investigation.

2.6. Cytotoxic activity

The cytotoxic aptitude of each afforded EtOAc extract was evaluated by the 3-[4,5-dimethylthiazol-2-yl]−2,5-diphenyltetrazolium bromide (MTT) assay (Hamed et al., 2021a) using cell lines of HepG-2 (hepatocellular carcinoma) and MCF-7 (breast cancer), which were previously obtained from VACSERA, Cairo, Egypt. Cells were initially cultured at 37 °C and incubated with 5% CO_2 using Dulbecco's Modified Eagle's Medium (DMEM)-high glucose (Invitrogen/Life Technologies, USA) inclosing 10% fetal bovine serum (FBS) (Hyclone, USA), along with 1% penicillin-streptomycin, thereafter, they were removed to 96-well plates with density of 2.2×10^4 cell/cm^2 and incubated overnight. Subsequently, each EtOAc extract was solubilized in dimethylsulfoxide (DMSO) and added to culture medium at different concentrations (20, 30, 40, 50, and 60 μg/mL). After 24 h, the viability of cells was estimated using MTT assay. Concisely, different treated cells with 150 μL/well of 0.5 mg/mL MTT reagent were incubated for 3 h at 37 °C, then dissolving of the consequent crystals were achieved by re-incubating them in 150 μL DMSO/well for 1 h at 37 °C protected from light. A microplate reader (ELx800, BioTek Instruments, VT) with BioTek's Gen5^{TM} data analysis software was used to measure the absorbance of each plate at 570 nm. Finally, DMSO was used to establish the viability baseline and the dose-response curve was consequently set to get the IC_{50} values. Doxorubicin (D1515, Sigma-Aldrich, Germany) was used herein as the positive control.

2.7. Topoisomerase I and topoisomerase II inhibition assays

The activity of DNA Topo I and Topo II (TopoGEN, Inc., Buena Vista, USA) was verified firstly through measuring the relaxation of supercoiled DNA pHOT1 and pRYG, respectively (Siwek et al., 2014). The reaction mixture was set following the manufacture's protocol (https://www.topogen.com). Camptothecin was employed as a Topo I inhibitor positive control, while Etoposide (VP-16) was contributed as an anti-Topo II positive control. Quantitative determination of topoisomerase activity was achieved by scanning the photographic negatives and evaluating the area displaying supercoiled DNA, which was transferred as a single band at the bottom of the gel by UVI-KS4000i gel documentation and analysis system (SyngenBiotech, Sacramento, CA). The inhibitor concentrations that prohibited converting of the fifty percent (IC_{50} values) of the supercoiled DNA into relaxed DNA were measured from dose response curve of at least five experiments.

2.8. Metabolic analysis

Chemical profile of the selected EtOAc extract was analysed using Triple Quadrupole Liquid Chromatograph Mass Spectrometer (LC-MS/MS) Shimadzu LC8050. Chromatographic separation was performed on ACE C18 column (Advanced Chromatography Technologies Ltd, Aberdeen, Scotland) with diameters of 4.5 × 75 mm and particle size of 5 μm Linear gradient elution of acetonitrile containing 0.1% formic acid (v/v) (eluent B) starting from 10% to 100%, with 0.3 mL/min flow rate., through 30 min and water as eluent A with 0.1% formic acid (v/v) was set, then 5 min an iscoctatic elution of 100% eluent B was set. Then the column was equilibrated again for 10 min at the initial mobile phase composition. One microliter was the injected volume of the sample and the column temperature was 25 °C. The resultant raw data were converted into sliced negative and positive ionization files by Shimadzu Labsolution software. Then, the attained files were submitted to the data mining MZmine 2.10 software (Okinawa Institute of Science and Technology Graduate University, Japan) with the purpose of peak picking, deconvolution, deisotoping, alignment, and formula prediction. The dereplication and characterization of compounds were achieved using available databases viz. Dictionary of Natural Products (DNP) and Metlin databases.

2.9. Docking study

A Processor Intel(R) Pentium(R) CPU N3510@ 1.99 GHz as well as Memory (4 GB) conjugated with Microsoft Windows 8.1 pro operating system (64 Bit) was used to perform the total calculations of molecular modeling and docking simulations through the computational software (Molecular Operating Environment (MOE 2019.0102, 2020; Chemical Computing Group, Canada). Total MOE minimizations were achieved until an RMSD gradient of 0.01 Kcal/mol/Å with the force field GBVI/WSA to calculate the partial charges automatically using a reaction field solvation. Previous to simulations, the LigX function was used to protonate the protein and the ligand was isolated. The 3D of Top I and II were acquired from Protein Data Bank (https://www. rcsb. org/; PDB ID codes: 1T8I (Staker et al., 2005) (topoisomerase I) 3QX3 (topoisomerase II) (Wu et al., 2011). The protein binding sites were managed using modules of Ligand Atoms Selection of MOE, and the camptothecin and etoposide binding sites were used in the crystal structure as references. The sequence order of the binding sites was set using the MOE program. The docking simulation process and the placement were managed on triangular matcher. The rescoring was managed on London dG parameter, and the conformation number was managed in 5 poses with 30 refinements; conformation was selected as the forcefield of MOE and was used to generate 5 poses. As the result of the docking run, the output file is in mdb form with the scoring of some conformations. All the docking conformations were analyzed, and the best value with the precise pose was selected for further interactional study.

2.10. Molecular dynamics (MD) simulations

The MD simulations for the docked complexs of the most promising compounds on the Topo I and Topo II receptors, compared to reference control complexs (CPT-Topo I and Etop-Topo II), were performed using the Desmond package (Schrödinger LLC) (El-Masry et al., 2022; Mahmoud et al., 2021; Release, 2017). The NPT ensemble with the temperature 300 K and a pressure 1 bar was applied in all runs. The simulation length was 100 ns with a relaxation time 1 ps for the ligands. The OPLS3 force field parameters were used in all simulations. The cutoff radius in Coulomb interactions was 9.0 Å. The orthorhombic periodic box boundaries were set 10 Å away from the protein atoms. The water molecules were explicitly described using the transferable intermolecular potential with three points (TIP3P) model. Salt concentration set to 0.15 M NaCl and was built using the System Builder utility of Desmond. The Martyna−Tuckerman−Klein chain coupling scheme with a coupling constant of 2.0 ps was used for the pressure control and the Nosé−Hoover chain coupling scheme for the temperature control. Nonbonded forces were calculated using a RESPA integrator where the short-range forces were updated every step and the long-range forces were updated every three steps. The trajectories were saved at 20 ns intervals for analysis. The behavior and interactions between the ligands and protein were analyzed using the Simulation Interaction Diagram tool implemented in Desmond MD package. The stability of MD simulations was monitored by looking on the RMSD of the ligand and protein atom positions in time (Abo Elmaaty et al., 2021; Alnajjar et al., 2020).

2.11. Statistical analysis

Statistical analysis was achieved by using GraphPad Prism 9 software (Version 9, San Diego, CA, USA). One-way analysis of variance (ANOVA) was performed. The obtained data was shown as mean ± standard error of mean.

3. Results

3.1. Morphological and molecular identification of the isolated endophytic fungal strain

The isolated endophytic fungal strain was identified and kept as *Aspergillus terreus* AArEF2 in Microbial Repository of Botany and Microbiology (MRBM) Department, Faculty of Science, Minia University, Minia, Egypt and stored at 4 °C. The growth of fungal strain was detected on PDA media as white mycelia colonies, which by time changed to brownish yellow. The microscopical feature of the investigated strain showed biseriate, compact and densely columnar conidial heads. It has smooth conidiophores and small, globose-shaped, and smooth-walled conidia. The ITS sequence obtained for the isolated fungal strain was sent to the GenBank for a homology search with BLAST. Alignment with existing published sequences in GenBank demonstrates 99% similarity of the isolated fungal strain with *Aspergillus terreus* AArEF2 (Fig. 1).

3.2. Cytotoxic activity

The cytotoxic activity of each EtOAc extracts afforded from the five different liquid growth media were investigated via MTT assay, using doxorubicin as a positive control. As demonstrated in Fig. 2, the EtOAc extract of MPDB media displayed remarkable growth inhibitory potential against HepG-2 and MCF-7 cell lines with IC_{50} values of 7.92 ± 0.03 and 8.53 ± 0.15 μg/mL, respectively as compared with doxorubicin. While, that of REB media showed potent cytotoxic aptitude versus MCF-7 cell line (IC_{50} = 6.94 ± 0.04 μg/mL) but moderately prohibited the growth of HepG-2 cell line (IC_{50} = 19.67 ± 0.15 μg/mL). On the other hand, the obtained extract from MREB media showed moderate cytotoxic potential against both tested cell lines (IC_{50} = 25.58 ± 0.04 and 30.7 ± 0.76 μg/mL for HepG-2 as well as MCF-7 cell lines, respectively). Contrary to the above-mentioned media extracts, the EtOAc extracts obtained from SAB and MEB media displayed very weak cytotoxic activities (IC_{50} > 100 μg/mL).

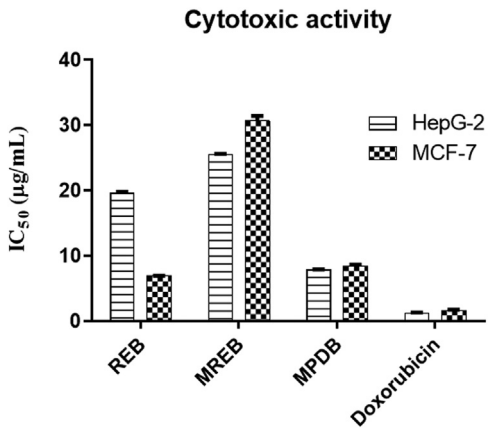

Fig. 2. Cytotoxic activities of the ethyl acetate extracts recovered from different media culture filtrates of *Aspergillus terreus* AArEF2.

3.3. Topoisomerase inhibition assay

The EtOAc extract afforded from MPDB media, which displayed the most potent cytotoxic potentials against both tested cell lines, was subjected to topoisomerase I & II inhibition assay (**Figs. S3** & **S4**). The Topoisomerase I inhibitor CPT successfully inhibited the topoisomerase activity as shown by the relaxed DNA band (**Fig. S3**). As samples were treated with protenase-K, one can also detect open circular DNA bands on the top of the gel further confirming the effect of the positive control drugsIn lanes 7–10, the tested extract inhibited the TOP I induced DNA relaxation. 100 μM of the extract effectively formed a nicked open circular DNA together with wiping out the relaxed DNA suggesting a mixed catalytic inhibitory and interfacial poisoning effects. Lower concentrations from the extract showed a nicked open circular DNA (faint bands on the top of the gel) with relaxed DNA. These nicked open circular bands are comparable in size and intensity with the bands shown in the positive control lanes further suggesting a similarity in the mechanism of action of both compounds (**Fig. S3**). Compared to the TOP I-treated substrate, all other bands in the positive control (CPT) and tested extract (MPDB) showed a reduction of the relaxed DNA and the formation of nicked open circular DNA bands in keeping with the mechanism of action of these poisons **Fig. S3**). Regarding topoisomerase II inhibition assay (**Fig. S4**), TOP II with DMSO together with the DNA substrate showed a perfect relaxation in supercoiled DNA. This TOP II induced relaxation was completely abolished by the Etoposide poison and the tested extract at higher doses. Moreover, both positive control (Etoposoide)

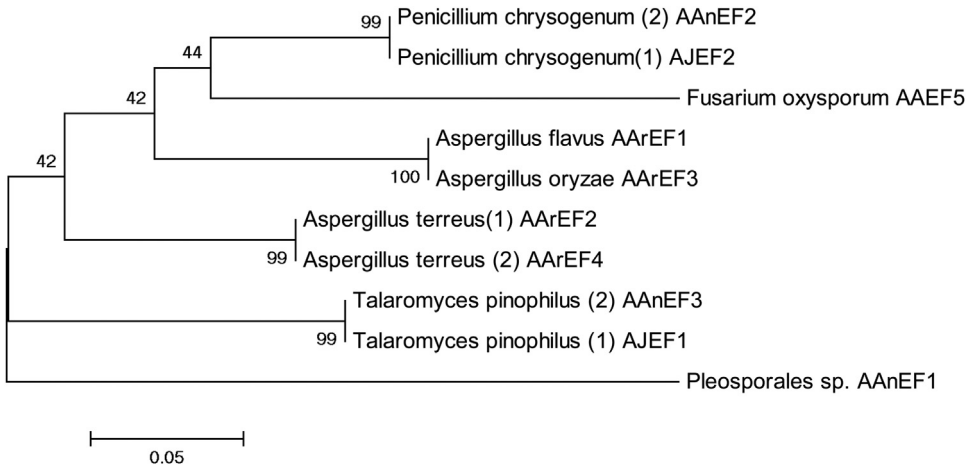

Fig. 1. Phylogenetic tree of the identified *Aspergillus terreus* AArEF2 strain isolated from *Artemisia arborescens* leaves (For interpretation of the references to color in this figure, the reader is referred to the web version of this article).

and the tested extract showed a dose dependent inhibition of the DNA relaxation as one would expect in this type of experiment. At lower doses of the drugs, one can detect the accumulation of the linear DNA. Finally, gel images (**Figs. S3** & **S4**) confirmed the dual enzyme-inhibitory and DNA cleavage action of the tested extract.

Moreover, the investigated extract revealed excellent topoisomerase II inhibitory potential with IC_{50} value of 2.83 ± 0.04 μg/mL, and was more potent than etoposide (IC_{50} = 5.81 ± 0.15 μg/mL), which was used as a positive control (Topo II poison). Nevertheless, its inhibitory activity towards topoisomerase I (IC_{50} = 8.76 ± 0.15 μg/mL), was lower than camptothecin (IC_{50} = 4.37 ± 0.76 μg/mL), which acted as a positive control (Topo I inhibitor).

3.4. Metabolomics study

Chemical analysis of the EtOAc extract afforded from MPDB media, displaying the most remarkable cytotoxic activities, was performed via the untargeted LC–ESI– HRMS metabolomics tool. Such analysis revealed the detection of numerous metabolites of which, 15 compounds were tentatively identified (Table 1 and Fig. 3). The negative and positive ionization mode data sets **(Figs. S1& S2)** of the inspected extract were dereplicated against available databases. The detected m/z 249.1492 $[M + H]^+$ for the predicted molecular formula (MF) $C_{15}H_{20}O_3$ was dereplicated as terrecyclic acid A (**1**) a tricyclic sesquiterpenoide. It was separated before from *A. terreus* and was reported for its antitumor activity against lymphocytic leukemia P388 (Nakagawa et al., 1982) as well as human lung cancer NCI-H460, MCF-7, and SF-268 (CNS glioma) cell lines (Wijeratne et al., 2003). The detected m/z 261.1128 $[M + H]^+$ for the proposed MF $C_{15}H_{16}O_4$ was identified as pseudodeflectusin (**2**), an antitumor isochroman derivative separated from A. pseudodeflectus (Ogawa et al., 2004). It demonstrated cytotoxic potentials versus a number of cancer cell lines (human cancer) comprising the stomach (NUGC-3), cervix (HeLa-S3), and peripheral blood (HL-60). Likewise, the detected m/z 263.1285 $[M + H]^+$ for the predicted MF $C_{15}H_{18}O_4$ was dereplicated as ustusorane A (**3**), a cytotoxic benzofuran derivative against human HL-60 cell line, which was previously reported from marine-derived *A. ustus* 094,102 (Liu et al., 2009). While, that at m/z 265.1436$[M-H]^-$ was annotated as 5(6)-dihydro-6-hydroxyterrecyclic acid A, (**4**) with the MF $C_{15}H_{22}O_4$. It was also reported from *A. terreus* with moderate cytotoxic potential towards NCI-H460, MCF-7 and SF-268 (Wijeratne et al., 2003). Another compound, with the MF $C_{15}H_{12}O_6$, was identified as funalenone (**5**), a phenalenone derivative, in harmony with the detected m/z 289.0713$[M + H]^+$. This compound was formerly obtained from *A. niger* FO-5904 and *A. tubingensi* (Inokoshi et al., 1999). Moreover, the detected m/z 295.2273 $[M + H]^+$, corresponding to the proposed MF $C_{18}H_{30}O_3$ was dereplicated as tetrahydro-6-(3-hydroxy-4,7-tridecadienyl)−2H-pyran-2-one (**6**), previously isolated from *A. nidulans* (Mazur et al., 1990). Additionally, the detected m/z 307.2274 $[M + H]^+$, for the suggested MF $C_{19}H_{30}O_3$ was dereplicated as dihydromonacolin L (**7**), which was previously isolated from *A. terreus* (Treiber et al., 1989). Similarly, the detected m/z 308.2225 $[M + H]^+$, in agreement with the MF $C_{18}H_{29}NO_3$, was dereplicated as viriditin (**8**) a pyrrolidine derivative compound, which was previously identified from *A. viridinutans* JO297 and showed weak cytotoxic properties against the cell line KB3.1 (Omolo et al., 2000). Moreover, the detected m/z 319.0818 $[M + H]^+$, corresponding to the MF $C_{16}H_{14}O_7$, was dereplicated as atrochrysone carboxylic acid (**9**), a polyketide derivative, which was previously reported from *A. terreus and A. nidulans* (Klejnstrup et al., 2012). Besides, the detected m/z 319.1540177 $[M-H]^-$ was dereplicated as betulinan A (**10**) with the MF $C_{20}H_{16}O_4$. It was earlier separated from *A. terreus* and showed moderate cytotoxic effects against NCI-H460, MCF-7 and SF-268 cell lines (Wijeratne et al., 2003). Another detected m/z 330.2067 $[M + H]^+$, was dereplicated as colchatetralene (**11**), with the MF $C_{18}H_{19}NO_5$. It was also separated from *Aspergillus* sp. and showed cytotoxic potential towards several human cancer cell lines such as A-549, MCF-7, CV-1, OVCAR-5 and THP-1 (Budhiraja et al., 2013). Furthermore, the predicted MF $C_{20}H_{20}O_7$ at m/z 371.1518 $[M-H]^-$, was distinguished as averantin (**12**), an anthraquinone derivative (Klejnstrup et al., 2012), formerly reported in *A. Versicolor*. This compound exhibited strong cytotoxicity against five human tumor cell lines (A549, SK-OV-3, SK-MEL-2, XF-498, and HCT-15) (Lee et al., 2010). Additionally, the detected 397.1674, with the MF $C_{24}H_{18}\ N_2O_4$ was dereplicated as asterriquinone D (**13**), a benzoquinone derivative that was earlier reported in *A. terreus* (Wijeratne et al., 2003). This metabolite exhibited cytotoxic activities against NCI-H460, MCF-7, and SF-268 cell lines. The cytotoxic metabolite, asterredione (**14**) with the MF $C_{24}H_{18}\ N_2O_5$ was also dereplicated from the detected m/z 415.3184083 $[M + H]^+$. This component was previously reported from *A. ochraceus* with selective cytotoxic potential versus human cancer cell lines including NCI-H460, SMMC-7721, and SW1990 (Cui et al., 2010). Finally, the detected m/z 455.2795 $[M + H]^+$ corresponding to the MF $C_{28}H_{40}O_5$, was dereplicated as 12,15,25,26-tetrahydroxyergosta-4,6,8(14),22-tetraen-3-one (**15**) which formerly obtained from *A. terreus* (Haritakun et al., 2012).

3.5. Docking studies of the dereplicated compounds

The fifteen compounds tentatively characterized from *A. terreus* AArEF2 were docked into the binding site of Top I and Top II and compared to camptothecin and etoposide which are co-assayed as positive controls (Tables 2 and 3). The interaction energies of compounds 1–15

Table 1
A list of the tentatively identified compounds from the EtOAc extract derived from MPDB.

NO	RT	*m/z*	Mode	Accurate mass	Calculated mass	Molecular formula	Putative identification	Chemical class
1	5.82	249.1492	P	248.1419	248.1412	$C_{15}H_{20}O_3$	Terrecyclic acid A	Sesquiterpene
2	7.47	261.1128	P	260.1055	260.1049	$C_{15}H_{16}O_4$	Pseudodeflectusin*	Isochroman
3	9.48	263.1285	P	262.1212	262.1205	$C_{15}H_{18}O_4$	Ustusorane A*	Benzofuran
4	6.99	265.1436	N	266.1509	266.1518	$C_{15}H_{22}O_4$.	5(6)-dihydro-6-hydroxyterrecyclic acid A	Sesquiterpene
5	8.06	289.0713	P	288.0641	288.0634	$C_{15}H_{12}O_6$	Funalenone*	Phenalenone
6	5.75	295.2273	P	294.2200	294.2195	$C_{18}H_{30}O_3$	Tetrahydro-6-(3-hydroxy-4,7-tridecadienyl)-2H-pyran-2-one*	Pyranone
7	9.32	307.2274	P	306.2201	306.2195	$C_{19}H_{30}O_3$	Dihydromonacolin L*	Pyranone
8	4.93	308.2225	P	307.2152	307.2147	$C_{18}H_{29}NO_3$	Viriditin*	Pyrrolidine
9	4.48	319.0818	P	318.0745	318.0740	$C_{16}H_{14}O_7$	Atrochrysone carboxylic acid	Polyketide
10	7.15	319.1540	P	320.1612	320.1049	$C_{20}H_{16}O_4$	Betulinan A	Quinone
11	8.51	330.2067	P	329.1994	329.1263	$C_{18}H_{19}NO_5$	Colchatetralene*	Pseudoalkaloid
12	12.60	371.1518	N	372.1591	372.1209	$C_{20}H_{20}O_7$	Averantin*	Anthraquinone
13	12.78	397.1674	N	398.1747	398.1267	$C_{24}H_{18}\ N_2O_4$	Asterriquinone D	Indole alk.
14	10.23	415.3184	P	414.3111	414.3134	$C_{24}H_{18}\ N_2O_5$	Asterredione*	Indole alk.
15	11.76	455.2795	N	456.2867	456.2876	$C_{28}H_{40}O_5$	12,15,25,26-Tetrahydroxyergosta-4,6,8(14),22-tetraen-3-one	Ergosterol

*Compounds identified for the first time from the A. terreus.

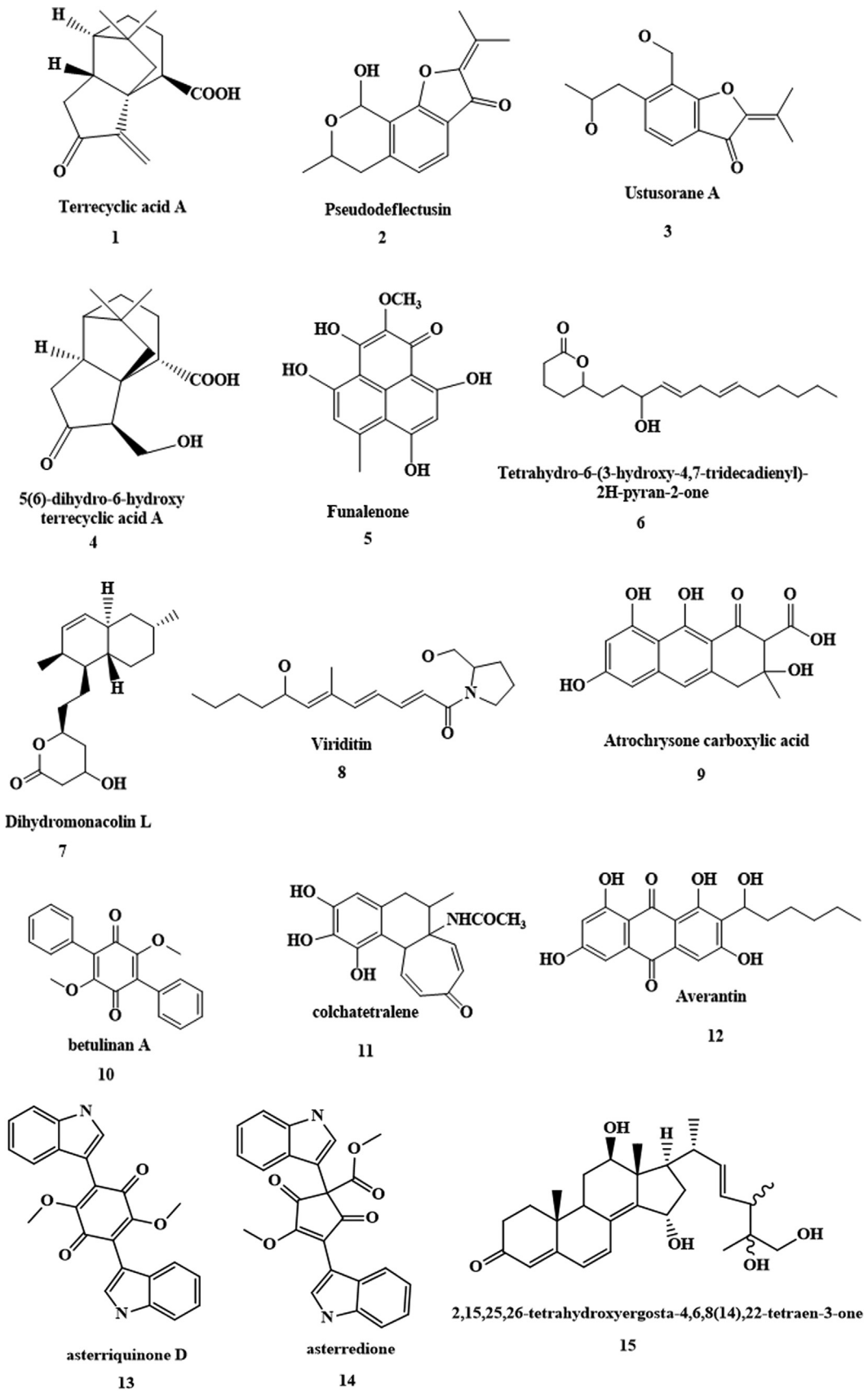

Fig. 3. Chemical structures of the dereplicated compounds of the EtOAc extract derived from Modified Potato Dextrose Broth (MPDB) culture filtrate of A. terreus AArEF2.

Table 2
The docking results of the target compounds 1–15 into camptothecin binding site of human topoisomerase I.

Compound NO.	S dG Kcal/mole	E_conf Kcal/mole	rmsd_refine	Receptor Amino acid/Type of bonding/Distance (Å) /Binding Energy (Kcal/mole)
12	−8.5714	−39.9471	1.7339	ARG 364 (A)/H-acceptor/3.03/−3.2 DA 113 (D)/pi-pi/3.76/−0.0 DC 112 (D)/pi-pi/3.92/−0.0 TGP 11 (C)/pi-pi/3.87/−0.0 TGP 11 (C)/pi-pi/3.48/−0.0
Camptothecin	−8.3632	74.9463	1.7123	ARG 364 (A)/H-acceptor/3.02/−4.8 LYS 425 (A)/H-acceptor/3.26/−2.3 DA 113 (D)/pi-pi/3.60/−0.0 TGP 11 (C)/pi-pi/3.44/−0.0 TGP 11 (C)/pi-pi/3.92/−0.0 DT 10 (B)/pi-pi/3.92/−0.0 TGP 11 (C)/pi-pi/3.85/−0.0
8	−8.1513	−7.2669	1.0350	TGP 11 (C)/H-pi/3.81/−0.5 TGP 11 (C)/H-pi/3.86/−0.5
15	−8.0361	47.6552	1.4943	DA 113 (D)/pi-pi/3.75/−0.0 TGP 11 (C)/pi-pi/3.44/−0.0 TGP 11 (C)/pi-pi/3.41/−0.0
13	−7.9843	138.2005	1.3501	DA 113 (D)/pi-pi/3.91/−0.0 TGP 11 (C)/pi-pi/3.65/−0.0 TGP 11 (C)/pi-pi/3.48/−0.0
14	−7.9146	97.0888	1.5372	LYS 425 (A)/H-acceptor/3.00/−5.2 TYR 426 (A)/pi-H/4.28/−0.5 DA 113 (D)/pi-pi/3.88/−0.0 DC 112 (D)/pi-pi/3.65/−0.0 DA 113 (D)/pi-pi/3.52/−0.0 DA 113 (D)/pi-pi /3.81/−0.0
10	−7.8697	74.9030	1.5055	HIS 632 (A)/pi-H/4.30/−0.7 TGP 11 (C)/pi-pi/3.63/−0.0 TGP 11 (C)/pi-pi/3.97/−0.0
5	−7.6613	28.1621	0.7722	ASN 722 (A)/H-donor/3.18/−1.3 TGP 11 (C)/pi-H/3.53/−0.5 DT 10 (B)/pi-pi/3.52/−0.0

(*continued*)

Table 2 (*Continued*)

Compound NO.	S dG Kcal/mole	E_conf Kcal/mole	rmsd_refine	Receptor Amino acid/Type of bonding/Distance (Å) /Binding Energy (Kcal/mole)
				TGP 11 (C)/pi-pi/3.74/−0.0 DA 113 (D)/pi-pi/3.89/−0.0 TGP 11 (C)/pi-pi/3.48/−0.0 TGP 11 (C)/pi-pi/3.50/−0.0
2	−7.4462	19.7697	1.3781	DC 112 (D) H-donor/2.91/−0.7 ARG 364 (A)/H-acceptor/3.05/−3.0 DA 113 (D)/pi-pi/3.77/−0.0 TGP 11 (C)/pi-pi/3.63/−0.0 TGP 11 (C)/pi-pi/3.56/−0.0 TGP 11 (C)/pi-pi/3.70/−0.0
9	−7.4027	−92.2096	1.8082	GLU 356 (A)/H-donor/2.87/−3.7 TGP 11 (C)/pi-pi/3.88/−0.0 TGP 11 (C)/pi-pi/3.69/−0.0
6	−7.3743	2.7372	1.1340	MET 428 (A)/H-acceptor/3.18/−1.3
11	−6.8873	−20.6025	0.9029	LYS 425 (A)/H-acceptor/2.89/−5.6 ARG 364 (A)/H-acceptor/3.16/−0.9 DA 113 (D)/pi-pi/3.96/−0.0
7	−6.6787	−28.8994	1.8694	–
3	−6.5928	42.0203	1.2097	GLU 356 (A)/H-donor/3.18/−0.9 ARG 364 (A)/H-acceptor/2.91/−4.6 TGP 11 (C)/H-pi/3.60/−0.7 DA 113 (D)/pi-pi/3.93/−0.0 DA 113 (D)/pi-pi/3.71/−0.0 TGP 11 (C)/pi-pi/3.91/−0.0 DC 112 (D)/pi-pi/3.97/−0.0
4	−5.7742	7.5329	1.8034	DA 113 (D)/H-donor/3.04/−1.7 DC 112 (D)/H-pi/4.24/−0.5
1	−5.6344	−1.6002	1.3894	LYS 425 (A)/H-acceptor/3.58/−0.8

S-The final score, rmsd_refine the root mean square deviation between the pose before refinement and the pose after refinement, E_conf-The energy of the conformer.

revealed that all compounds showed rmsd-refine values less than the value 2 indicating that the investigated compounds bind inside the pockets of camptothecin and etoposide (Figs. 4–7). Compound (**12**) named averantin showed higher **S**_score binding energy (−8.5714 kcal per mole) than that of CPT (−8.3632 kcal per mole). Compounds **8, 15,**

Table 3
The docking results of the target compounds 1–15 into etoposide binding site of human top II.

Compound NO.	S	E_conf	rmsd_refine	Receptor
	dG Kcal/mole	Kcal/mole		Amino acid/Type of bonding/Distance (A)/Binding Energy (Kcal/mole)
Etoposide	−8.7513	58.8835	1.8434	ASP 479 (A)/H-donor/ 3.53/−0.6 ARG 503 (A)/pi-H/4.25/ −0.7 DG 13 (F)/pi-pi/3.93/ −0.0
14	−7.5239	99.5734	1.7660	ASP 479 (A)/H-donor/ 2.98/−7.5 DG/10 (D) pi-H/4.76/ −0.5 DT 9 (D)/pi-pi/3.65/−0.0
15	−7.2112	26.2794	2.0192	DT 9 (D)/H-pi/3.95/−1.3 DT 9 (D)/H-pi/3.85/−0.6
13	−7.2056	134.9363	1.8912	DG 13 (F)/H-pi/4.25/ −0.5 ARG 503 (A)/pi-H/4.49/ −0.5
7	−7.1722	−27.3783	0.9919	ASP 479 (A)/H-donor/ 3.30/−1.2 ARG 503 (A)/pi-H/4.23/ −0.8 ASP 479 (A)/H-donor/ 3.02/−1.6 ASP 479 (A)/H-acceptor/ 3.03/−1.5
6	−6.7791	−9.1149	1.6133	–
10	−6.6780	76.8671	1.5454	–
11	−6.6389	16.3658	1.3528	ASP 479 (A)/H-donor/ 3.13/−1.5
8	−6.5554	−15.1898	1.0568	DG 10 (D)/H-donor/ 3.10/−0.7
12	−6.5540	−39.2241	1.7892	ARG 503 (A)/H-donor/ 2.97/−0.8 ASP 479 (A)/H-acceptor/ 3.05/−1.3 DT 9 (D)/H-pi/4.38/−0.6
3	−6.3278	38.8992	1.5353	DA 12 (F)/H-pi/4.12/ −0.6 ARG 503 (A)/pi-H/4.60/ −0.5
9	−6.2908	−90.6830	1.7930	DG 10 (D)/H-donor/ 3.10/−4.5 ASP 479 (A)/H-donor/ 2.95/−2.5
2	−6.1299	17.5085	1.2038	ARG 503 (A)/pi-H/4.00/ −1.2 ARG 503 (A)/pi-H/4.25/ −0.5
5	−5.8421	29.9669	0.9130	DA 12 (F)/pi-pi/3.99/ −0.0
1	−5.6899	−2.6945	1.1493	DG 13 (F)/H-pi/4.17/ −0.8 DA 12 (F)/H-pi/3.89/ −0.7
4	−5.2549	38.6155	1.9126	DT 9 (D)/H-donor/2.99/ −0.6 DT 9 (D)/H-acceptor/ 3.31/−0.7 DA 12 (F)/H-pi/4.58/−0.7

S-The final score, rmsd_refine-The root mean square deviation between the pose before refinement and the pose after refinement, E_conf-The energy of the conformer.

13, 14, 10, 5, 2, 9 and **6** displayed binding energies of 97.5–88.17% while, compounds **11, 7, 3, 4** and **1** showed moderate binding energies of 82.35–67.37% as compared to CPT. Averantin (**12**) showed π- π binding interactions with DNA especially with DA113 (D), DC112 (D), TGP11(C) and TGP11(C) in a manner very similar to CPT. It is good to mention that, these π- π interactions of the CPT drug with DNA were directly responsible for its stable ternary complex with Topo I. Also, averantin (**12**) was similar to CPT in the formation of hydrogen bonding with ARG364 (A). It is worth noting, that all compounds showed many other types of hydrogen bonding in addition to π- π binding and other hydrophobic bonds with the DNA and Topo I. Interestingly, compounds **12, 9, 11, 7** and **8** showed E_conf −39.9471, −92.2096, −20.6025, −28.8994, and −7.2669 kcal/mole, respectively and were better than that of CPT which showed E_conf 74.9463 kcal/mole to reveal their higher affinity to the Topo I binding site than that of CPT. Furthermore, etoposide and the fifteen dereplicated compounds (**1**–**15**) were docked into the etoposide binding site. The results revealed that etoposide exhibited the highest binding energy score (−8.5714). Compounds **14, 15, 13** and **7** showed 85.97–81.96% of binding energy, respectively as compared to the etoposide. Compounds **6, 10, 11, 8, 12, 3, 9**, and **2** showed moderate score of binding energy (77.46–70.05%), while compounds **5, 1** and **4** were the lowest in score of binding energies (66.76–60.05%) as compared to etopside. On the other hand, compound **9** showed E_conf energy −90.6830, which is comparatively superior to that of etoposide (−58.8835). Compounds **7, 6, 8, 12**, and **1** showed E-conf −27.3783, −9.1149, −15.1898, −39.2241, and −2.6945, respectively, which are better than that of etoposide. Moreover, compounds **14, 11, 12, 9, 7** showed hydrogen bonding with ASP479 (A) in a manner similar to etoposide. Also, many compounds and etoposide as well, showed H-π bonding with ARG 503 (A). Most compounds showed variable π-π or H-π interactions with the DNA nucleotides like DG/10 (D), DT 9(D), DG13 and DA12 (F).

Furthermore, to confirm the docking results and give more details concerning the thermodynamic behaviors of the most promising compounds (**12** and **14**), molecular dynamics simulations were carried out as well. The docked complex of the most promising compound on the Topo I receptor (**12**-Topo I) was compared to its reference control complex (CPT-Topo I). Also, the docked complex of the most promising candidate on Topo II receptor (**14**-Topo II) was compared to its reference control complex (Etoposide-Topo II).

3.6. Molecular dynamics (MD) simulations

The MD simulations were carried out to evaluate the stability of the most promising docked complexes (**12**-Topo I, CPT-Topo I, **14**-Topo II, and Etoposide-Topo II) in physiological conditions. The MD simulations were performed for 100 ns.

3.6.1. RMSD analysis

The Root Mean Square Deviation (RMSD) was considered to study the degree of deviation quantitatively from the initial structure throughout the simulation time.

Regarding the RMSD of Topo I complexes we can observe that the **12**-Topo I complex fluctuated within the range of (0–5.4 Å) while the CPT-Topo I one fluctuated within the range of (0–3.4 Å), (Fig. 8**A**). On the other hand, concerning the RMSD of Topo II complexes, we can find that the **14**-Topo II complex fluctuated within the range of (0–5 Å) while the Etoposide-Top II complex fluctuated within the range of (0–4.5 Å), (Fig. 8**C**).

The RMSD of each ligand regarding to its initial position inside the active sites of both Topo I and Topo II proteins was recorded as a function of simulation time in Fig. 8**B** and **D**.

The ligand **12** of the **12**-Topo I complex showed a very stable interaction within the protein pocket from the start till the end of the simulation time. However, the reference CPT ligand of CPT-Topo I complex showed an initial deviation from 0 to 20 ns till it returned to the deep pocket of Topo I receptor till the end of the simulation time (Fig. 8**B**).

Furthermore, ligand **14** of **14**-Topo II complex showed great stability within the receptor pocket throughout the time of the simulation. Besides, the reference Etoposide ligand of the Etopoposide-Topo

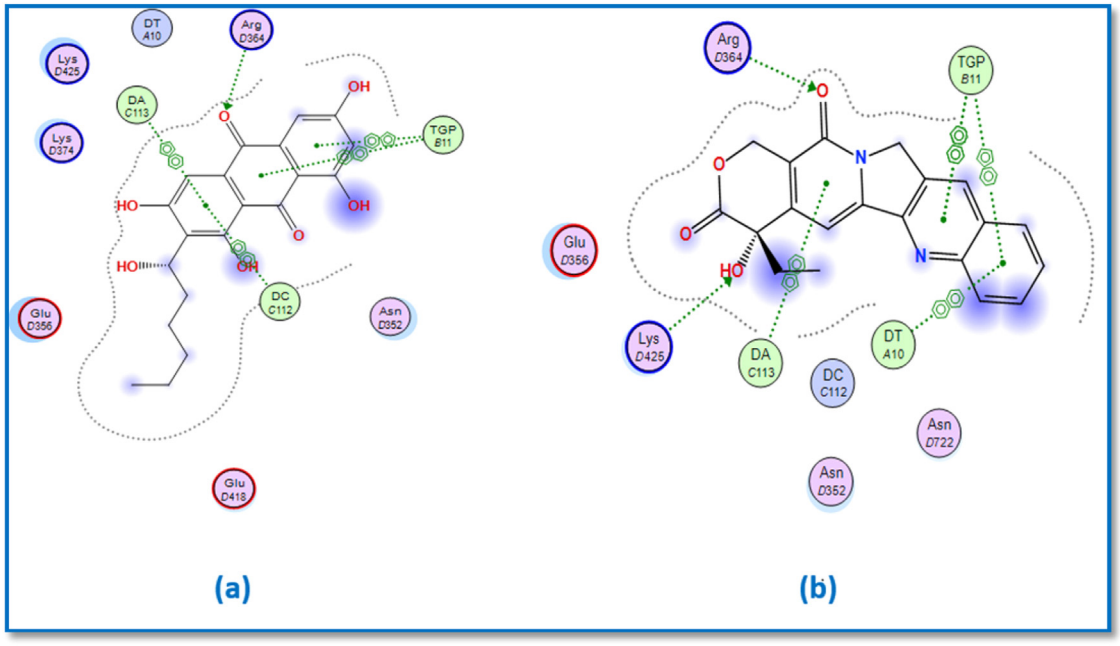

Fig. 4. 2D representation of docking of compound 12 (a) and CPT (b) into CPT binding site of Topo I.

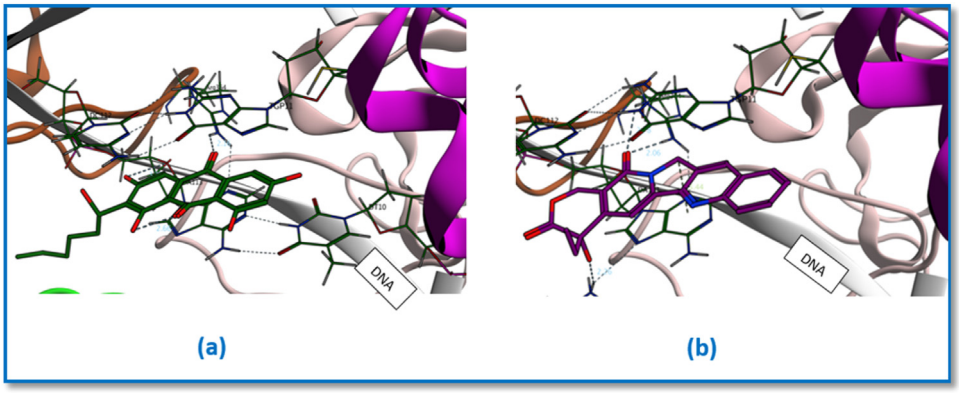

Fig. 5. 3D representation of docking of compound 12 (a) and CPT (b) into camptothecin binding site in Topo I.

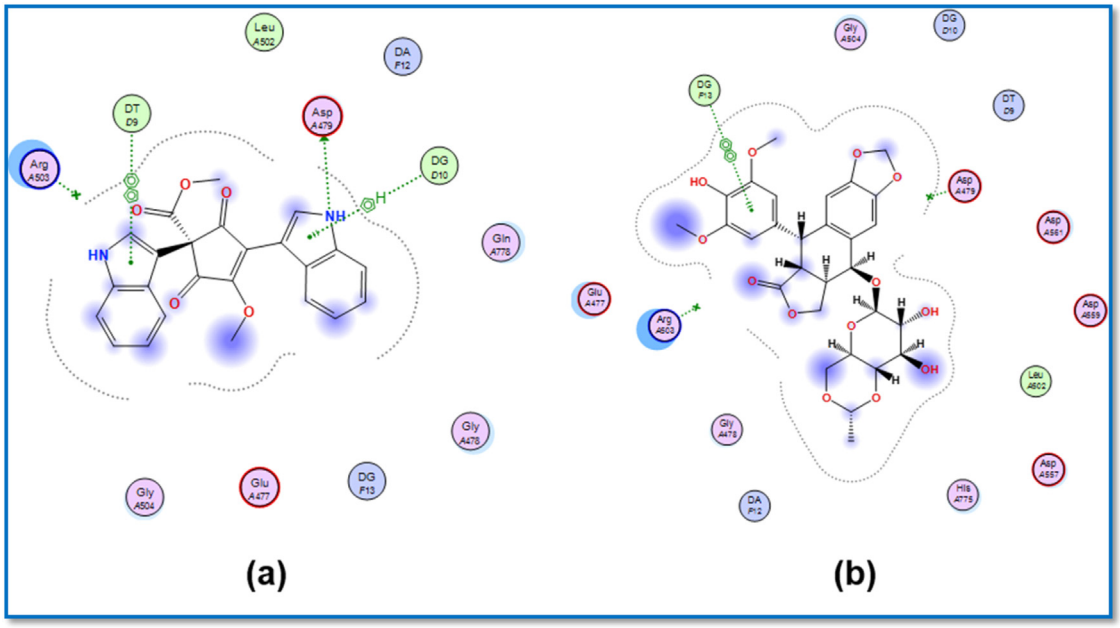

Fig. 6. 2D representation of docking of compound 14 (a) and etoposide (b) into etoposide binding site in Topo II.

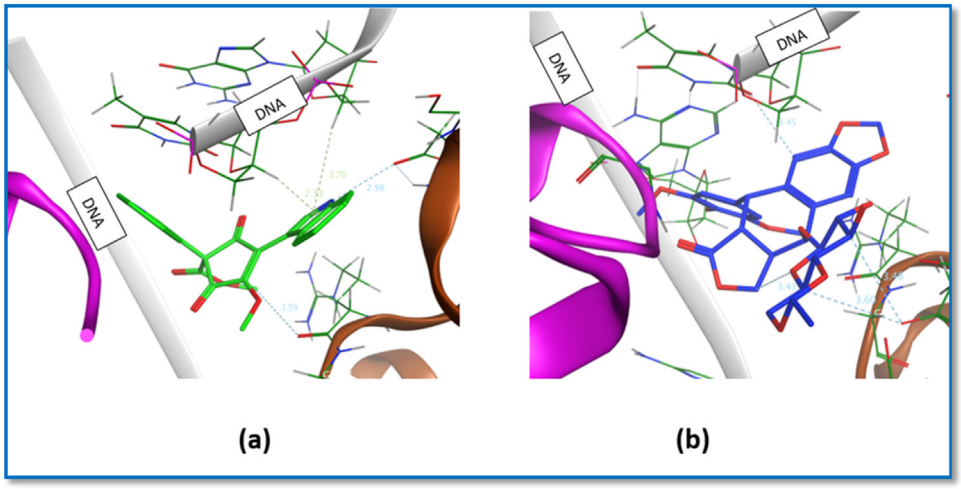

Fig. 7. 3D representation of docking of compound 14 (a) and etoposide (b) into etoposide binding site in Topo II.

II complex showed a small deviation outside the deep receptor pocket from 10 to 50 ns before it returned to the deep pocket till the end of the simulation time (Fig. 8**D**). Based on the above, we can conclude the great stability of both compounds **12** and **14** towards the Topo I and Topo II receptor pockets, respectively, which was found to be superior to that of their reference standards.

3.6.2. *RMSF analysis*

The Root Mean Square Fluctuation (RMSF) was studied to evaluate the local changes within the protein structure that occur due to the presence of the described inhibitor. This gives more information about the flexibility of the protein receptor all over the simulation time. The RMSFs of both Topo I proteins were around 5.5 and 6.5 Å for **12**-Topo I and CPT-Topo I complexes, respectively. The largest fluctuations were observed from 450 to 500 residues in both complexes (Fig. 9**A**). However, the RMSFs of both Topo II proteins were around 6.2 and 5.8 Å for **14**-Topo II and Etoposide-Topo II complexes, respectively. There are two observed large fluctuations between 150 and 200 residues for both complexes as well (Fig. 9**B**).

3.6.3. *Binding interactions histogram and heat map analysis*

To describe the protein-ligand binding interactions in more detail, the histogram was discussed for each one of the studied complexes all over the 100 ns of the simulation as depicted in Fig. 10.

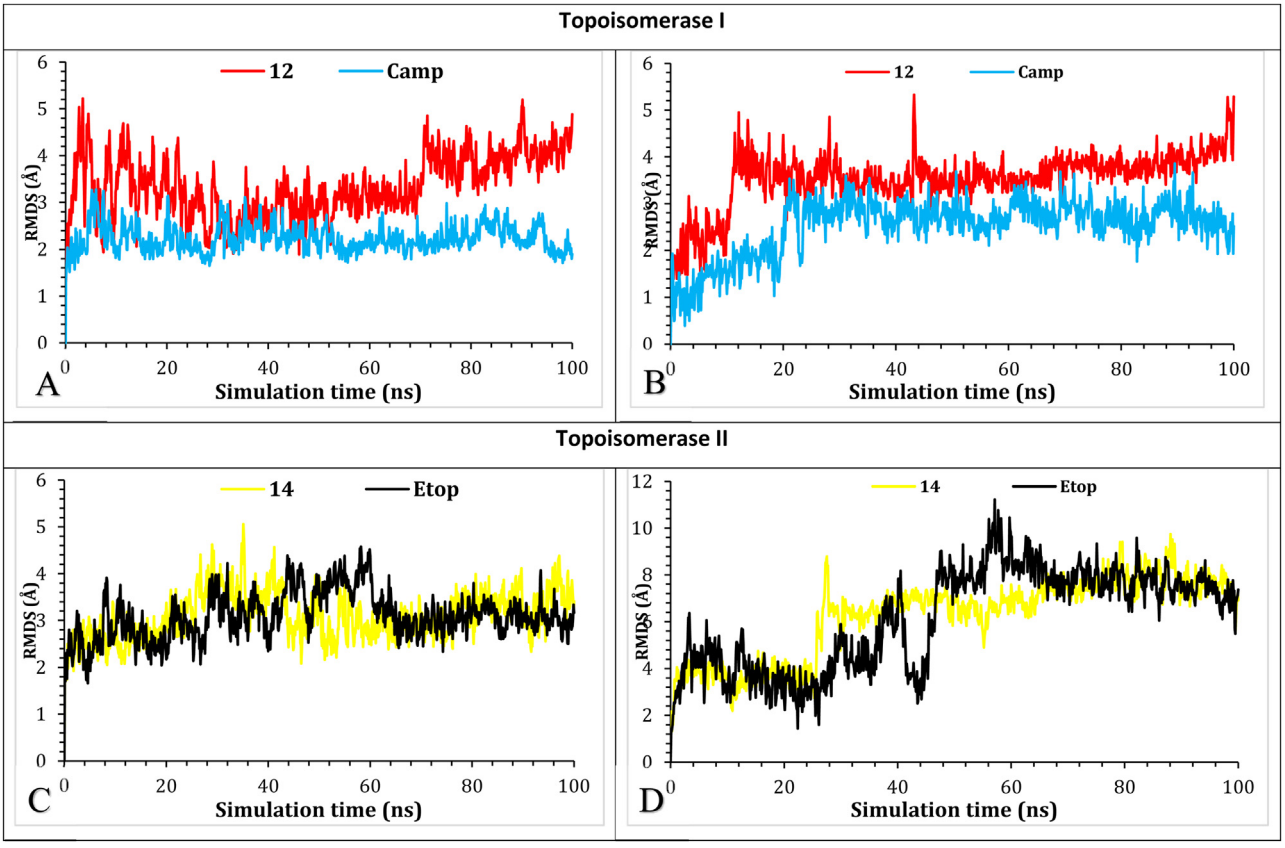

Fig. 8. The RMSD of the protein (A and C) and the protein-ligand complexes (B and D) for Topo I and Topo II proteins, respectively, as a function of simulation time (100 ns).

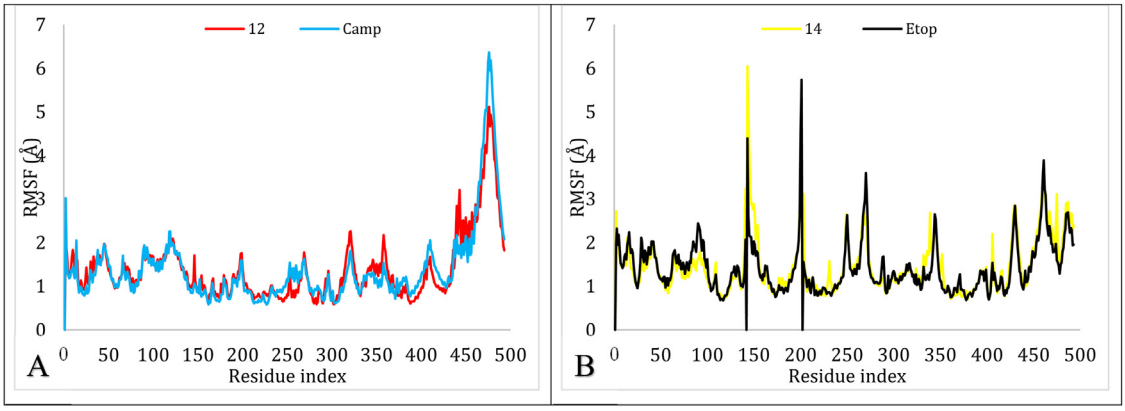

Fig. 9. The RMSF of the Topo I protein (A) and the Topo II protein (B).

Studying the **12**-Topo I complex histogram, it was found that both Glu356 and Arg364 amino acids of the receptor pocket contributed mainly to the interactions to compound **12** with 100% and 60% interactions fraction, respectively. Both amino acids contributed through H-bonds and H_2O-bridged H-bonds, however, Arg364 contributed also by ionic bonds (Fig. 10**A**). on the other hand, the CPT-Topo I complex histogram showed that Asn352 was the most amino acid contributing to the interactions with the reference ligand (> 150%) through H-bonds and H_2O-bridged H-bonds (Fig. 10**B**). Moreover, the histogram of the **14**-Topo II complex clarifies that Lys505 amino acid interactions were the most contributing with > 100% through H_2O-bridged H-bonds mainly and small H-bonds interactions (Fig. 10**C**). Finally, the Etoposide-Topo II complex histogram showed that both Arg503 and Asp479 amino acids contributed mainly by > 70% and > 50%, respectively, to the reference ligand interactions. The contributions of Arg504 were through H-bonds, hydrophobic, and H_2O-bridged H-bonds. However, those of Asp479 were through H-bonds, ionic, and H_2O-bridged H-bonds (Fig. 10**D**).

The heat maps were represented in Fig. 11 to describe the total number of interactions for the studied inhibitors within their receptor pockets compared to the reference standards.

Regarding the **12**-Topo I complex, it was noted that Glu356 amino acid contributed in the interactions all over the simulation time with more ligand contacts after 50 ns till the end of the simulation. However, the Arg364 contributions were mainly from the start till 50 ns (Fig. 11**A**). Moreover, the heat map of the CPT-Topo I complex showed that Asn352 contributed to the ligand interactions all over the simulation time with more contributions from 20 ns till the end

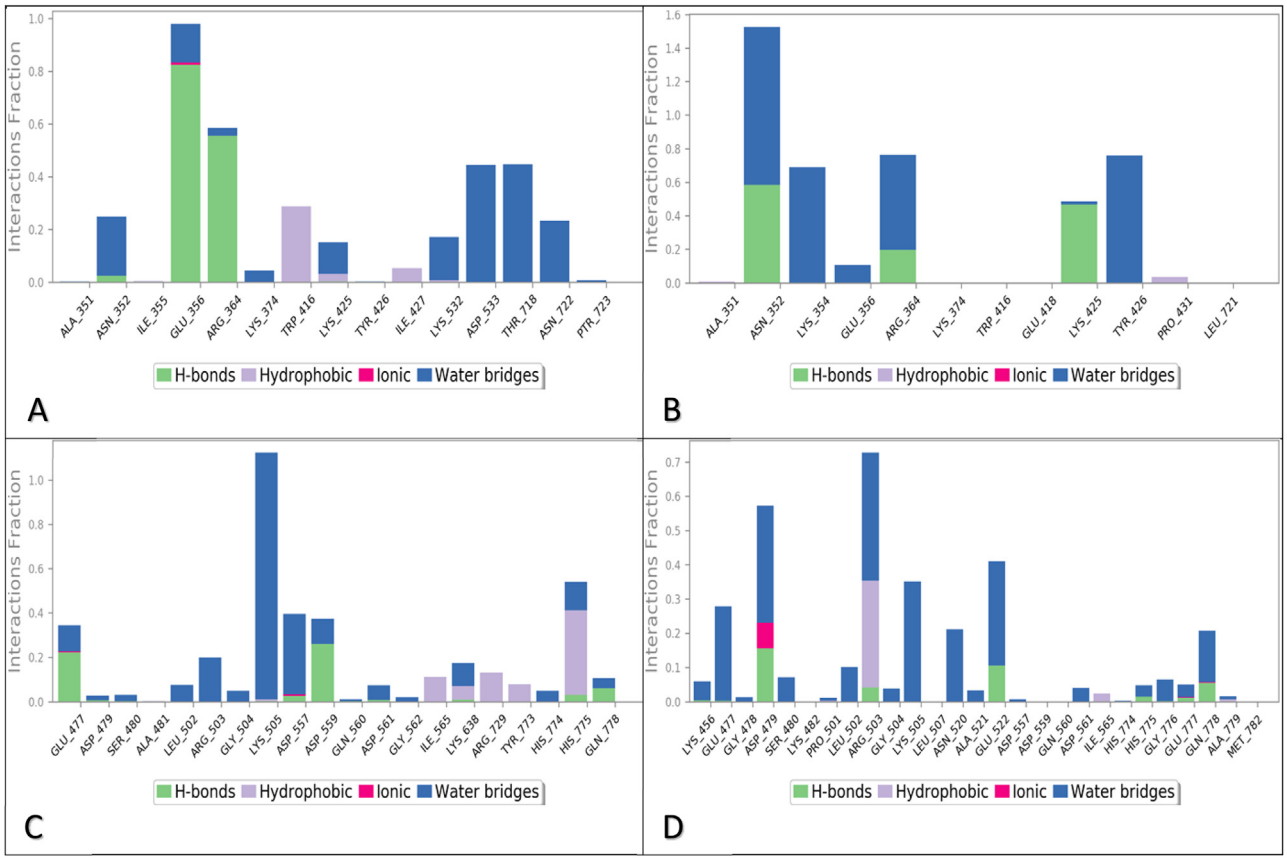

Fig. 10. Histogram describing the binding interactions between the protein and its ligand during the simulation time of 100 ns for (A) 12-Topo I, (B) CPT-Topo I, (C) 14-Topo II, and (D) Etoposide-Topo II.

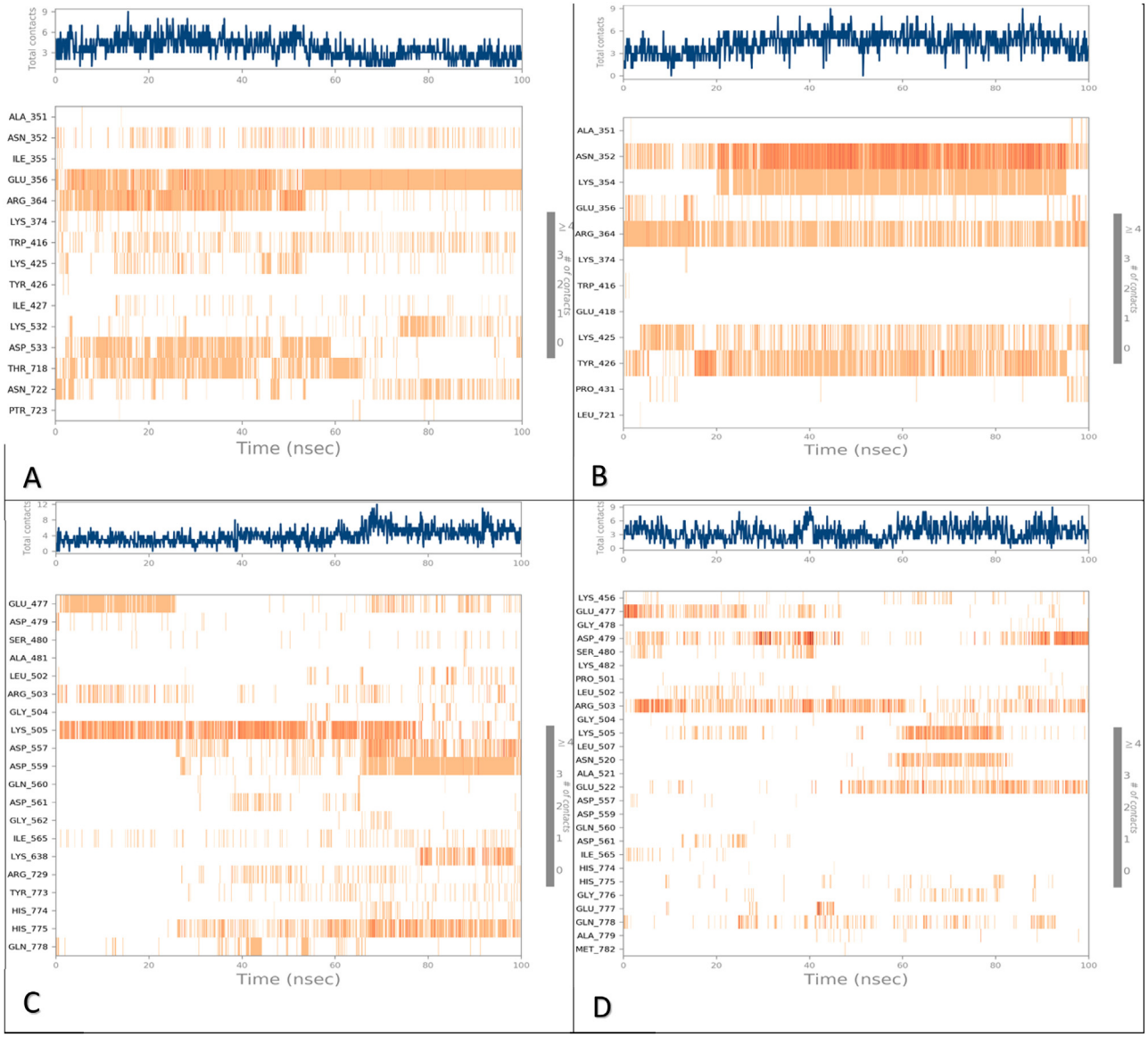

Fig. 11. Heat map showing the total number of protein-ligand interactions all over the simulation time of 100 ns for (A) 12-Topo I, (B) CPT-Topo I, (C) 14-Topo II, and (D) Etoposide-Topo II.

of the simulation time (Fig. 11**B**). Also, the **14**-Topo II complex heat map showed that Lys505 amino acid contacts were mainly from the start till 80 ns of the simulation time (Fig. 11**C**). Finally, the heat map of the Etoposide-Topo II complex clarified that Arg503 amino acid contributions were mainly from the start till 60 ns and Asp479 amino acid contributions were mainly from (0–40 and 80–100 ns) of the simulation time (Fig. 11**D**).

4. Discussion

As consequences of the therapeutic relevance of metabolites afforded from the endophytic fungi, the cultivation of fungi on different media to afford various metabolites has found its way into a large array of pharmaceutical uses, resulting in a remarkable production of endophyte related compounds, that might be potential anticancer drug leads. Recent scientific efforts have, therefore, displayed the potential of such natural products produced from the endophytic fungi for multiple medicinal applications as well as good resources of alternative cytotoxic agents (Uzma et al., 2018). In this sense, such work gave the opportunity to dig into the chemical constituents and biological potentials of the *A. terreus* AArEF2 strain isolated from the leaves of *A. arboresscens*. As yet, the chemical profile of *Aspergillus* species has been considerably studied as a superior source of numerous bioactive leads represented by butenolides, terpenoids, alkaloids, phenalenones, r-terphenyls, diphenyl ether, cytochalasins, sterols, anthraquinone, and xanthones derivatives. Such metabolites are mainly responsible for various reported biological activities of *Aspergillus* species, such as anticancer, antimicrobial, antiviral, antitrypanosomal, antileishmanial, and anti-inflammatory potentials (Elhawary et al., 2020). *Aspergillus terreus*, in particular, is well-known by bioactive metabolites obtained from its culture fermentation on different media, such as sterols, butenolides, alkaloids, and meroterpenoids, of which some are reported with cytotoxic potentials (Elhawary et al., 2020). In this context, findings of the current study of *A. terreus* AArEF2 fermented on MBDP liquid culture revealed its capacity to accumulate various classes of secondary metabolites (Table 1), encompassing sesquiterpenes, isochroman, benzofuran, phenalenone, pyranones, pyrrolidine, polyketide, quinone, pseudoalkaloid, indol alkaloids, anthraquinone, and sterol. LC-ESI-HRMS based-metabolomics configured the chemical profile of the

endophytic microorganisms, where nine metabolites were identified tentatively, herein, for the first time from *A. terreus* (Table 1), while the others, comprising terrecyclic acid A (**1**), 5(6)-dihydro-6-hydroxyterrecyclic acid A (**4**), atrochrysone carboxylic acid (**9**), betulinan A (**10**), asterriquinone D (**13**), and 12,15,25,26-tetrahydroxyergosta-4,6,8(14),22-tetraen-3-one (**15**) were earlier reported from this species. Conforming with the US NCI guidelines, the antitumor findings interestingly revealed the strong (IC50 < 20 μg/mL) to moderate (IC50 = 21–50 μg/mL) cytotoxic potential of *A. terreus* towards the HepG-2 and MCF-7 cell lines; a result that highlight on the anticancer potential of such isolated fungal strain. Concerning the characterized components of the respective extract (MPDB), its noteworthy cytotoxic activities versus HepG-2 and MCF-7 cell lines might be ascribed to the presence of metabolites namely, terrecyclic acid A (**1**), pseudodeflectusin (**2**), ustusorane A(**3**), viriditin (**8**), betulinan A (**10**), colchatetralene (**11**), averantin (**12**) and asterredione (**14**) with cytotoxicity aptitudes in line with previously reported data (Cui et al., 2010; Klejnstrup et al., 2012; Liu et al., 2009; Nakagawa et al., 1982; Ogawa et al., 2004; Omolo et al., 2000; Wijeratne et al., 2003) thus, it proposes the involvement of such compounds to the anticancer capacity of the investigated *A. terreus* AArEF2. Despite the reported cytotoxic properties of such compounds, no previous reports have addressed their possible molecular cytotoxic mechanisms, and the investigation of their topoisomerase inhibitory activity is still unexplored. By studying the activity of the EtOAc extract of MPDB culture filtrate on topioomerase enzymes, it displayed remarkable enzymes inhibition potentials comparable to the positive controls (Fig. 3 and 4). Cancer is thought to be a genetic disease resulting from gene mutations, that are related to cell proliferation leading to DNA damage. Cancer comprehension has uncovered numerous new targets for the evolution of effective therapies. Gene therapies, which aim to directly attack the tumor cells, are thought to achieve their goals, but many obstacles should be first overcome before approving their clinical trials (Luo et al., 2009). On the other side, conventional therapies based on radiotherapy, surgery, chemotherapy have various adverse effects, because normal cells are not protected from their destructive effects. Recently, drug resistance is considered one of the major problems in cancer therapy which may arise from modification at any step in the cell apoptotic pathway of the antitumor drug targets (Bertram, 2000). DNA topoisomerases are considered the marvelous molecular tools by which the topology of DNA in a cell could be stated through managing the problems associated with the replication, transcription, and translation of the DNA. They could temporarily break a DNA strand or a couple of complementary strands and pass other single or double-stranded segments. Such enzymes are also reported to bring about many interconversions such as catenation, knotting, decatenation, and unknotting (Baikar and Malpathak, 2010). Lack of sensitivity to different topoisomerase I and II inhibitors has been reported in tissue culture cells associated with overexpression of Multidrug Resistance Mutation (MDR1); decreased levels of topoisomerase, drug-resistant mutant topoisomerase, elongation of cell cycle time, and changes in DNA repair functions. Consequently, an alternative source for the cancer treatment is warranted (Chen and Liu, 1994). In this context, the identified metabolites of the investigated strain, based on LC—HRMS tool, were assessed by *in silico* molecular docking on Topo I and Topo II to recognize their potential inhibitors. Docking poses and binding energies were compared to well-known inhibitors, such as CPT and etoposide as anti-topoisomerase I and II, respectively. The obtained docking results displayed molecular interactions of almost all dereplicated compounds with Topo I and Topo II binding sites showing remarkable binding affinities in comparison to CPT and etoposide, particularly averantin (**12**) and asterredione (**14**) (Tables 2 and 3) recommending that the cytotoxic aptitude of the docked metabolites from *A. terreus* AArEF2 are mediated by inhibition of Topo I and Topo II. Moreover, the MD simulations for 100 ns of the most promising candidates (**12** and **14**) on the target receptors (Topo I and Topo II), respectively, confirmed greatly the docking results. Surprisingly, the stability of both mentioned compounds exceeded that of their reference standards as well.

5. Conclusion

Considering the promising potential of *A. terreus* as a source of auspicious alternates for cancer treatment, the cytotoxic potentials of the EtOAc extracts derived from its fermentation on different culture media were investigated and the most active cytotoxic one was assayed for its ability to inhibit topoisomerase, hence its chemical characterization was also addressed. The EtOAc extract derived from MPDB culture filtrate showed noteworthy *in vitro* cytotoxic action against liver and breast cancer cells and remarkable Topo I and Topo II inhibitory activities, which have been attributed to its various metabolites. Molecular docking analysis of such metabolites highlighted their topoisomerases inhibitory capacity as a prospective mechanism of their cytotoxicity, particularly averantin (**12**) and asterredione (**14**) which demonstrated promising interaction abilities with Topo I and Topo II binding sites, respectively as compared to positive control drugs.The docking results were confirmed by molecular dynamics simulations for 100 ns, that give more details concerning the thermodynamic behaviors of the mentioned compounds within the physiological conditions as well. Consequently, these findings might validate the promising use of endophytic *A. terreus* AArEF2 strain isolated from *A. arborescens* as a source of different phytochemicals with possible chemotherapeutic applications.

Declaration of Competing Interest

The authors declare there is no conflict of interest.

Acknowledgments

We thank Minia and Deraya Universities for supporting this work

References

Abo Elmaaty, A., Hamed, M.I.A., Ismail, M.I., Elkaeed, E.B., Abulkhair, H.S., Khattab, M., Al-Karmalawy, A.A., 2021. Computational insights on the potential of some NSAIDs for treating COVID-19: priority set and lead optimization. Molecules 26, 3772.

Alhadrami, H.A., Sayed, A.M., El-Gendy, A.O., Shamikh, Y.I., Gaber, Y., Bakeer, W., Sheirf, N.H., Attia, E.Z., Shaban, G.M., Khalifa, B.A., Ngwa, C.J., Pradel, G., Rateb, M.E., Hassan, H.M., Alkhalifah, D.H.M., Abdelmohsen, U.R., Hozzein, W.N., 2021. A metabolomic approach to target antimalarial metabolites in the *Artemisia annua* fungal endophytes. Sci. Rep. 11, 2770.

Alnajjar, R., Mostafa, A., Kandeil, A., Al-Karmalawy, A.A.J.H., 2020. Molecular docking, molecular dynamics, and *in vitro* studies reveal the potential of angiotensin II receptor blockers to inhibit the COVID-19 main protease. Heliyon 6, e05641.

Andrews, S., Pitt, J., 1986. Selective medium for isolation of Fusarium species and *dematiaceous hyphomycetes* from cereals. Appl. Environ.Microbiol. 51, 1235–1238.

Attia, E.Z., Farouk, H.M., Abdelmohsen, U.R., El-Katatny, M.M.H., 2020. Antimicrobial and extracellular oxidative enzyme activities of endophytic fungi isolated from alfalfa (*Medicago sativa*) assisted by metabolic profiling. S. Afr. J. Bot. 134, 156–162.

Baikar, S., Malpathak, N., 2010. Secondary metabolites as DNA topoisomerase inhibitors: a new era towards designing of anticancer drugs. Pharmacogn. Rev. 4, 12–26.

Baldwin, E.L., Osheroff, N., 2005. Etoposide, topoisomerase II and cancer. Curr. Med. Chem. Anticancer Agents 5, 363–372.

Barnett, H., Hunter, B., 1972. Illustrated Genera of Imperfect Fungi. Burgess Publishing Company, Minneapolis, Minnesota.

Bertram, J.S., 2000. The molecular biology of cancer. Mol. Asp. Med. 21, 167–223.

Budhiraja, A., Nepali, K., Sapra, S., Gupta, S., Kumar, S., Dhar, K.L., 2013. Bioactive metabolites from an endophytic fungus of Aspergillus species isolated from seeds of *Gloriosa superba* Linn. Med. Chem. Res. 22, 323–329.

Buzun, K., Bielawska, A., Bielawski, K., Gornowicz, A., 2020. DNA topoisomerases as molecular targets for anticancer drugs. J. Enzyme Inhib. Med. Chem. 35, 1781–1799.

Champoux, J.J., 2001. DNA topoisomerases: structure, function, and mechanism. Annu. Rev. Biochem. 70, 369–413.

Chen, A.Y., Liu, L.F., 1994. DNA topoisomerases: essential enzymes and lethal targets. Annu. Rev. Pharmacol. Toxicol. 34, 191–218.

Corley, D.G., Durley, R.C., 1994. Strategies for database dereplication of natural products. J. Nat. Prod. 57, 1484–1490.

Cui, C.M., Li, X.M., Meng, L., Li, C.S., Huang, C.G., Wang, B.G., 2010. 7-Nor-ergosterolide, a pentalactone-containing norsteroid and related steroids from the marine-derived endophytic *Aspergillus ochraceus* EN-31. J. Nat. Prod. 73, 1780–1784.

El-hawary, S.S., Moawad, A.S., Bahr, H.S., Abdelmohsen, U.R., Mohammed, R., 2020. Natural product diversity from the endophytic fungi of the genus Aspergillus. RSC Adv. 10, 22058–22079.

El-Masry, R., Al-Karmalawy, A.A., Alnajjar, R.A., Mahmoud, S., Mostafa, A., Kadry, H., Abou-Seri, S., Taher, A., 2022. Newly synthesized series of oxoindole-oxadiazole conjugates as potential Anti-SARS-CoV-2 agents: *in silico* and *in vitro* studies. New J. Chem.. https://doi.org/10.1039/D1NJ04816C.

Elebeedy, D., Badawy, I., Elmaaty, A.A., Saleh, M.M., Kandeil, A., Ghanem, A., Kutkat, O., Alnajjar, R., Abd El Maksoud, A.I., Al-karmalawy, A.A., 2021a. *In vitro* and computational insights revealing the potential inhibitory effect of tanshinone IIA against influenza A virus. Comput. Biol. Med. 141, 105149.

Elebeedy, D., Elkhatib, W.F., Kandeil, A., Ghanem, A., Kutkat, O., Alnajjar, R., Saleh, M.A., Abd El Maksoud, A.I., Badawy, I., Al-Karmalawy, A.A., 2021b. Anti-SARS-CoV-2 activities of tanshinone IIA, carnosic acid, rosmarinic acid, salvianolic acid, baicalein, and glycyrrhetinic acid between computational and *in vitro* insights. RSC Adv. 11, 29267–29286.

Elmaaty, A.A., Darwish, K.M., Chrouda, A., Boseila, A.A., Tantawy, M.A., Elhady, S.S., Shaik, A.B., Mustafa, M., Al-karmalawy, A.A., 2022. *In silico* and *in vitro* studies for benzimidazole anthelmintics repurposing as VEGFR-2 antagonists: novel mebendazole-loaded mixed micelles with enhanced dissolution and anticancer activity. ACS Omega 7, 875–899.

Gouda, S., Das, G., Sen, S.K., Shin, H.S., Patra, J.K., 2016. Endophytes: a treasure house of bioactive compounds of medicinal importance. Front. Microbiol. 7, 1538 1538.

Hamed, A.N.E., Abdelaty, N.A., Attia, E.Z., Amin, M.N., Ali, T.F.S., Afifi, A.H., Abdelmohsen, U.R., Desoukey, S.Y., 2021a. Antiproliferative potential of *moluccella laevis* L. aerial parts family lamiaceae (labiatae), supported by phytochemical investigation and molecular docking study. Nat. Prod. Res. 36, 1391–1395.

Hamed, M.I.A., Darwish, K.M., Soltane, R., Chrouda, A., Mostafa, A., Abo Shama, N.M., Elhady, S.S., Abulkhair, H.S., Khodir, A.E., Elmaaty, A.A., Al-karmalawy, A.A., 2021b. β-Blockers bearing hydroxyethylamine and hydroxyethylene as potential SARS-CoV-2 Mpro inhibitors: rational based design, *in silico, in vitro*, and SAR studies for lead optimization. RSC Adv. 11, 35536–35558.

Haritakun, R., Rachtawee, P., Komwijit, S., Nithithanasilp, S., Isaka, M., 2012. Highly conjugated ergostane-type steroids and aranotin-type diketopiperazines from the fungus *Aspergillus terreus* BCC 4651. Helv. Chim. Acta 95, 308–313.

Inokoshi, J., Shiomi, K., Masuma, R., Tanaka, H., Yamada, H., Omura, S., 1999. Funalenone, a novel collagenase inhibitor produced by *Aspergillus niger*. J Antibiot. 52, 1095–1100 (Tokyo).

Jalgaonwala, R., Mohite, B.V., Mahajan, R., 2017. A review: natural products from plant associated endophytic fungi. J. Microbiol. Biotech. Res. 1, 21–32.

Klejnstrup, M.L., Frandsen, R.J.N., Holm, D.K., Nielsen, M.T., Mortensen, U.H., Larsen, T.O., Nielsen, J.B., 2012. Genetics of polyketide metabolism in *Aspergillus nidulans*. Metabolites 2, 100–133.

Krushkal, J., Negi, S., Yee, L.M., Evans, J.R., Grkovic, T., Palmisano, A., Fang, J., Sankaran, H., McShane, L.M., Zhao, Y., O'Keefe, B.R., 2021. Molecular genomic features associated with *in vitro* response of the NCI-60 cancer cell line panel to natural products. Mol. Oncol. 15, 381–406.

Kumar, S., Stecher, G., Tamura, K., 2016. MEGA7: molecular evolutionary genetics analysis version 7.0 for bigger datasets. Mol. Biol. Evol. 33, 1870–1874.

Lee, Y.M., Li, H., Hong, J., Cho, H.Y., Bae, K.S., Kim, M.A., Kim, D.K., Jung, J.H., 2010. Bioactive metabolites from the sponge-derived fungus *Aspergillus versicolor*. Arch. Pharm. Res. 33, 231–235.

Liu, H., Edrada-Ebel, R., Ebel, R., Wang, Y., Schulz, B., Draeger, S., Müller, W.E.G., Wray, V., Lin, W., Proksch, P., 2009. Drimane sesquiterpenoids from the fungus *Aspergillus ustus* isolated from the marine sponge *Suberites domuncula*. J. Nat. Prod. 72, 1585–1588.

Luo, J., Solimini, N.L., Elledge, S.J., 2009. Principles of cancer therapy: oncogene and non-oncogene addiction. Cell 136, 823–837.

Mahmoud, A., Mostafa, A., Al-Karmalawy, A.A., Zidan, A., Abulkhair, H.S., Mahmoud, S.H., Shehata, M., Elhefnawi, M.M., Ali, M.A., 2021. Telaprevir is a potential drug for repurposing against SARS-CoV-2: computational and *in vitro* studies. Heliyon 7, e07962.

Malonne, H., Atassi, G., 1997. DNA topoisomerase targeting drugs: mechanisms of action and perspectives. Anticancer Drugs 8, 811–822.

Mathers, C.D., Loncar, D., 2006. Projections of global mortality and burden of disease from 2002 to 2030. PLoS Med. 3, e442 e442.

Mazur, P., Meyers, H.V., Nakanishi, K., El-Zayat, A.A.E., Champe, S.P., 1990. Structural elucidation of sporogenic fatty acid metabolites from *aspergillus nidulans*. Tetrahedron Lett. 31, 3837–3840.

Nakagawa, M., Hirota, A., Sakai, H., Isogai, A., 1982. Terrecyclic acid A, a new antibiotic from Aspergillus terreus. I. Taxonomy, production, and chemical and biological properties. J. Antibiot. 35, 778–782 (Tokyo).

Nitiss, J.L., 2009a. DNA topoisomerase II and its growing repertoire of biological functions. Nat. Rev. Cancer 9, 327–337.

Nitiss, J.L., 2009b. Targeting DNA topoisomerase II in cancer chemotherapy. Nat. Rev. Cancer 9, 338–350.

Ogawa, A., Murakami, C., Kamisuki, S., Kuriyama, I., Yoshida, H., Sugawara, F., Mizushina, Y., 2004. Pseudodeflectusin, a novel isochroman derivative from Aspergillus pseudodeflectus a parasite of the sea weed, *Sargassum fusiform*, as a selective human cancer cytotoxin. Bioorg. Med. Chem. Lett. 14, 3539–3543.

Omolo, J.O., Anke, H., Chhabra, S., Sterner, O., 2000. New variotin analogues from *Aspergillus viridi-nutans*. J. Nat. Prod. 63, 975–977.

Prajapati, J., Goswami, D., Rawal, R.M., 2021. Endophytic fungi: a treasure trove of novel anticancer compounds. Curr. Res. Pharmacol. Drug Discov. 2, 100050.

Rasheed, Z.A., Rubin, E.H., 2003. Mechanisms of resistance to topoisomerase I-targeting drugs. Oncogene 22, 7296–7304.

Release, S., 2017. 3: Desmond Molecular Dynamics System, DE Shaw Research, New York, NY, 2017. Maestro-Desmond Interoperability Tools. Schrödinger, New York, NY.

Sak, K., 2012. Chemotherapy and dietary phytochemical agents. Chemother. Res. Pract. 2012, 282570.

Sashidhara, K.V., Rosaiah, J.N., 2007. Various dereplication strategies using LC-MS for rapid natural product lead identification and drug discovery. Nat. Prod. Commun. 2, 1934578X0700200218.

Singh, S., Sharma, B., Kanwar, S.S., Kumar, A., 2016. Lead phytochemicals for anticancer drug development. Front. Plant Sci. 7, 1667 1667.

Siwek, A., Bielawska, A., Maciorkowska, E., Lepiarczyk, M., Bielawski, K., Trotsko, N., Wujec, M., 2014. Cytotoxicity and topoisomerase I/II inhibition activity of novel 4-aryl/alkyl-1-(piperidin-4-yl)-carbonylthiosemicarbazides and 4-benzoylthiosemicarbazides. J. Enz. Inhib. Med. Chem. 29, 243–248.

Staker, B.L., Feese, M.D., Cushman, M., Pommier, Y., Zembower, D., Stewart, L., Burgin, A.B., 2005. Structures of three classes of anticancer agents bound to the human topoisomerase I-DNA covalent complex. J. Med. Chem. 48, 2336–2345.

Treiber, L.R., Reamer, R.A., Rooney, C.S., Ramjit, H.G., 1989. Origin of monacolin L from Aspergillus terreus cultures. J. Antibiot. 42, 30–36 (Tokyo).

Uzma, F., Mohan, C.D., Hashem, A., Konappa, N.M., Rangappa, S., Kamath, P.V., Singh, B.P., Mudili, V., Gupta, V.K., Siddaiah, C.N., Chowdappa, S., Alqarawi, A.A., Abd Allah, E.F., 2018. Endophytic fungi-alternative sources of cytotoxic compounds: a review. Front. Pharmacol. 9, 309.

Wang, J.C., 2002. Cellular roles of DNA topoisomerases: a molecular perspective. Nat. Rev. Mol. Cell. Biol. 3, 430–440.

Wijeratne, E.M., Turbyville, T.J., Zhang, Z., Bigelow, D., Pierson, L.S., VanEtten, H.D., Whitesell, L., Canfield, L.M., Gunatilaka, A.A., 2003. Cytotoxic constituents of *Aspergillus terreus* from the rhizosphere of *Opuntia versicolor* of the Sonoran Desert. J. Nat. Prod. 66, 1567–1573.

Wu, C.C., Li, T.K., Farh, L., Lin, L.Y., Lin, T.S., Yu, Y.J., Yen, T.J., Chiang, C.W., Chan, N.L., 2011. Structural basis of type II topoisomerase inhibition by the anticancer drug etoposide. Science 333, 459–462.